Nuclear Inst. and Methods in Physics Research B 470 (2020) 10–14

Contents lists available at ScienceDirect

Nuclear Inst. and Methods in Physics Research B

journal homepage: www.elsevier.com/locate/nimb

Ab initio calculations of pure and Co^{+2}-doped MgF_2 crystals

A.B. Usseinov[a,*], D. Gryaznov[b,*], A.I. Popov[a,b,*], E.A. Kotomin[b,*], D. Seitov[c], F. Abuova[a], K.A. Nekrasov[c], A.T. Akilbekov[a]

[a] L.N. Gumilyov Eurasian National University, Munaitpassov Str. 5, 0100008 Nur-Sultan, Kazakhstan
[b] Institute of Solid State Physics, University of Latvia, 8 Kengaraga Str., Riga LV-1063, Latvia
[c] Ural Federal University, Yekaterinburg, Russia

ARTICLE INFO

Keywords:
MgF_2
Cobalt dopant
Ab initio
Fluoride

ABSTRACT

Ab initio calculations of the atomic, electronic and vibrational structure of a pure and Co^{+2} doped MgF_2 crystals were performed and discussed. We demonstrate that Co^{+2} ($3d^7$) ions substituting for Mg is in the high spin state. In particular, the role of exact non-local exchange is emphasized for a proper reproduction of not only the band gap but also other MgF_2 bulk properties. It allows us for reliable estimate of the dopant energy levels position in the band gap, and its comparison with the experimental data. Thus, the present *ab initio* calculations and experiment data demonstrate that the Co^{+2} ground state level lies at ≈2 eV above the valence band top.

1. Introduction

Magnesium fluoride (MgF_2) is a material highly transparent over an extremely wide range of photon energies, ranging from vacuum ultraviolet to infrared [1–4]. Therefore, it found a lot of applications in the different optical devices (e.g. lenses, filter, windows, laser elements) photocathodes as well as luminescent detectors [5–12]. A great variety of dopant ions and host lattices have been explored as candidates, and numerous examples of actual working lasers have been found [7,8,13–16]. Among them, lasers based on d^3 or d^7ions doped into ionic lattices are interesting for their tunability and high-temperature performance. Cobalt ions as a dopant belongs to this family, while MgF_2 belongs to the rutile family. The vibronic laser systems based on Co-doped MgF_2 are unique, because it has been demonstrated to lase efficiently, in a range of energies between 1960 and 2080 nm of practical interest. For practical long-term applications, it is also important to know and understand the properties of radiation defects and processes that have been studied and discussed in [17–21].

Since a detailed knowledge of the general spectral properties of the materials is necessary for better understanding of the optical and laser properties, we have performed here *ab initio* calculations of pure and Co-doped MgF_2

2. Details of calculations

Large-scale *ab initio* calculations have been performed using the linear combination of atomic orbitals (LCAO) formalism and Gaussian basis set (BS) as implemented in the CRYSTAL14 computer code [22]. It appeared in the present study that the choice of the exchange-correlation functional plays a crucial role. Thus, we are concerned on the comparison of several hybrid functionals for an accurate description of the basic properties of MgF_2. Namely, PBE0 [23] and HSE06 [24] which are widely used in the density functional calculations have been tried by us and compared. Moreover, we varied the amount of exact exchange (α mixing parameter) in the form

$$E_{XC}^{PBEh\alpha} = E_{XC}^{PBE} + \alpha(E_X^{HF} - E_X^{PBE}) \quad (1)$$

where E_{XC}^{PBE} the exchange-correlation part due to the standard PBE functional, E_X^{HF} the exact exchange part due to the Hartree-Fock method, E_X^{PBE} the exchange part due to the standard PBE functional. One can easily understand that Eq. (1) transforms to PBE0 [23] for $\alpha = 0.25$. In the present study α was varied in a wide range, from 0 to 0.45. As can be seen from the analysis below, the functional, i.e. E_{XC}^{PBEh45} gives better band gap and other properties of the crystal lattice of MgF_2 in a comparison with the experiment and other hybrid functionals. In the calculations with the HSE06 functional the length scale separation of 0.11 $Å^{-1}$ was applied.

The BS optimization was done in two steps: first, the BS of Mg and F in pure MgF_2 was re-optimized, and second, the BS of Mg, F, and Co was re-optimized in Co^{+2}-doped MgF_2. The basis sets (BSs) for Mg and F atoms were taken from Refs. [25] and [26], respectively, while that for Co atom taken from refs. [27,28] and were re-optimized with new functional set (PBEh45, exponents of Gaussian type orbitals smaller than 0.9 $Bohr^{-2}$ were re-optimized). Thus, we are concerned only with

* Corresponding authors.
E-mail addresses: usseinov_ab@enu.kz (A.B. Usseinov), gryaznov@mail.com (D. Gryaznov), popov@latnet.lv (A.I. Popov), kotomin@latnet.lv (E.A. Kotomin).

https://doi.org/10.1016/j.nimb.2020.02.038
Received 21 January 2020; Received in revised form 29 February 2020; Accepted 29 February 2020
Available online 12 March 2020
0168-583X/

Table 1
The exponents of Gaussian type orbitals (Bohr^{-2}) before and after optimization of the BS with the PBEh45 functional in pure MgF_2 crystal.

Type of orbital	Before	After
	Mg	
sp	0.688	0.659
sp	0.280	0.278
	F	
sp	0.450	0.419
sp	0.205	0.157

Table 3
Elastic coefficients c_{ij} and bulk modulus B in GPa of MgF_2. PBEh25 corresponds to the PBE0 functional.

	PBEh45	PBEh25	HSE06	Expt [38]
B	104.2	97.22	97.12	106.2
c_{11}	147.5	137.3	136.7	145.6
c_{12}	94.8	87.9	90.2	95.2
c_{13}	58.5	54.8	54.5	67.0
c_{33}	220.1	206.5	201.8	214.2
c_{44}	64.0	60.1	58.5	58.3
c_{66}	103.5	96.08	97.0	103.8

the virtual orbitals and their contraction, in a comparison to original BS (Table 1). The BS optimization of pure MgF_2 led to an energy gain of ~ 0.06 eV per primitive unit cell.

For SCF procedure, the high accuracies 10^{-8}, 10^{-8}, 10^{-8}, 10^{-8}, 10^{-16} have been chosen for calculations of the Coulomb overlap, Coulomb penetration, exchange overlap, first exchange pseudo-overlap and second exchange pseudo-overlap integrals, respectively. Total energy difference between two SCF steps (10^{-8} a.u.) also has a high tolerance of accuracy. Effective atomic charges have been estimated using the Mulliken population analysis [29]. The Monkhorst-Pack [30] k-points grid sampling was set as 6 × 6 × 6 for a primitive unit cell of MgF_2. We employ the so-called *supercell approach* [31], and perform the present calculations for the neutral supercells. To model doping of MgF_2 with the Co atom in the oxidation state +2 (Co^{+2}), we have considered the 96 atom supercell with one Mg ion replaced by one Co ion. Consequently, the 2 × 2 × 2 **k**-point mesh was accommodated. The relevant defect concentration was 3.1 at.%. The high-frequency dielectric constant using the coupled perturbed HF/Kohn-Sham method [32,33,34] and the frozen phonon method (direct method) for the calculation of vibrational frequencies as implemented in CRYSTAL code were used.

3. Perfect bulk MgF_2

MgF_2 has a rutile structure (space group $P4_2/mnm$) with 6 atoms per primitive unit cell. Table 2 shows the calculated lattice parameters (a, c, u), static and high-frequency dielectric constants (ε^0, ε^∞), effective atomic charge (q_{eff}) and band gap (E_g) of an MgF_2 crystal together with experimental data. The lattice parameters a,c for the PBEh45 functional agree much better with the experimental values. However, the free parameter u is insensitive to the functional. The calculated effective atomic charges demonstrate a quite ionic character of bonding in MgF_2 which is the effect less sensitive to the functional chosen as well. However, some degree of covalency is also seen from their values which makes MgF_2 different from MgO. In the latter case the effective atomic charge of Mg +1.91e if calculated with the hybrid B3LYP functional [22].

As can be seen in Table 2, the commonly used B3PW and PBEh25 hybrid functionals underestimate the band gap (9.50 and 9.84 eV, respectively) while the experimental value is 12.4–13.0 eV (Table 2). Increase of the amount of exact non-local exchange to α = 0.45 provided the value (12.57 eV) consistent with the experiments. As is known, a correct description of the band structure, in particular the band gap, is very important for positioning the energy levels of defects inside the forbidden gap. An important role of the band gap was often discussed in the literature [35,36], a scissor operator is widely used in the calculations, in order to obtain agreement with the experiments. Therefore, in our work, we have chosen the PBEh45 functional (Eq. (1)) for the calculations of defects levels in the band gap.

In addition to the basic electronic properties, we calculated also the elastic properties [40] (Table 3) and the phonon frequencies at the Γ-point of the Brillouin zone (Table 4, Table 5). An increase of the exact exchange percentage (the PBEh45 functional) leads to an improvement in the description of the bulk modulus and elastic coefficients, in a comparison with the experimental data. In the rutile structure the cation occupies the Wyckoff position 2a: (0, 0, 0) whereas the anion occupies the Wyckoff positons 4f: (u, u, 0). The set of optical phonon modes at the Γ-point is $\Gamma = 2a_{2u} + 4e_u + b_{1g} + b_{2g} + a_{1g} + e_g + 2b_{1u} + a_{2g}$. Among them one pair is silent, namely $2b_{1u} + a_{2g}$, and another pair $a_{2u} + e_u$ is acoustic. Only infra-red active phonon frequencies at the Γ-point are slightly overestimated by the PBEh45 functional in a comparison with both the experiment and PBEh25 functional. It is, however, reflected in the values of dielectric constants as the values of ε^0_{xx} and ε^0_{zz} are larger for the PBEh25 functional than those for the PBEh45 functional.

Thus, having tested the PBEh45 functional for the description of various properties of a pure MgF_2 crystal, we came to a conclusion on the importance of increased amount of exact non-local exchange (α in Eq. (1)). Note that not only the band gap but also other properties are better reproduced with the PBEh45 functional. Thus, the variation of α has been shown to have an important effect in the literature. To our knowledge, these studies concerned the HSE06 functional mainly. So, α for the HSE06 functional was varied in the calculations of bulk properties of perovskites [41] and bulk and reduction properties of CeO_2 [42]. Oba et al. [43] showed that the larger amount of exact non-local exchange, i.e. α = 0.375, is required to re-produce the band gap of

Table 2
Basic bulk properties of MgF_2 calculated with the hybrid functionals. PBEh25 corresponds to the standard PBE0 functional. a, c, u the lattice parameters, E_g the band gap, ε^∞_{xx}, ε^∞_{zz} the high-frequency dielectric constants, ε^0_{xx}, ε^0_{zz} the static dielectric constant, and q_{eff} the effective atomic charges due to Mulliken analysis. Notice the coupled perturbed HF/Kohn-Sham method used for the calculation of dielectric constants is implemented for HSE06 functional in the CRYSTAL code.

	PBEh45	PBEh25	HSE06	B3PW [37]	Expt
a, Å	4.604	4.648	4.627	4.654	4.615 [38]
c, Å	3.091	3.120	3.106	3.139	3.043 [38]
u(Fluorine)	0.43	0.43	0.43	–	0.3030 [38]
E_g, *eV*	**12.57**	9.84	11.17	9.50	12.4 [2] 13.0 [17]
ε^∞_{xx}	1.54	1.60	–	–	1.9 [39]
ε^∞_{zz}	1.58	1.64	–	–	1.9 [39]
ε^0_{xx}	4.52	4.62	–	–	5.4 [39]
ε^0_{zz}	3.75	3.91	–	–	4.6 [39]
q_{eff} (Mg/F), e	+1.765/−0.883	+1.748/−0.874	+1.761/−0.880	–	–

Table 4
Infra-red active phonon frequencies (in cm^{-1}) at the Γ-point of MgF_2 crystal. Measured phonon frequencies are taken from [39]. PBEh25 corresponds to the PBE0 functional.

Symmetry	PBEh45	PBEh25	Experiment
	Transverse (TO)		
b_{1u}	230	224	Silent
e_u	269	262	247
a_{2u}	427	411	399
e_u	434	422	410
b_{1u}	453	435	Silent
e_u	479	461	450
	Longitudinal (LO)		
e_u	331	320	303
e_u	435	424	415
e_u	662	641	617
a_{2u}	656	635	625

Table 5
Raman-active phonon frequencies (in cm^{-1}) at the Γ-point of MgF_2 crystal. Measured phonon frequencies are taken from [39]. PBEh25 corresponds to the PBE0 functional.

Symmetry	PBEh45	PBEh25	Experiment
b_{1g}	117	119	92
e_g	307	294	295
a_{2g}	336	325	Silent
a_{1g}	427	411	410
b_{2g}	528	511	515

ZnO. Nevertheless, Kuzmin et al. [44] showed that α in Eq. (1) is reduced to 0.13 leading to accurate lattice parameters, band gap and phonon frequencies in $CuWO_4$. Moreover, it was suggested in the literature [45] that $\alpha = 0.33$ in Eq. (1) reproduces much better the atomization and dissociation energies, bond lengths and excitation energies for corresponding datasets in comparison with the PBEh25 functional.

4. Co^{+2} doped MgF_2

When Co ion occupies a regular Mg lattice site (Fig. 1) its oxidation state is +2 in the neutral supercell. Let us consider a regular CoF_6 octahedron for simplicity. In an octahedral field the energy levels of Co^{+2} $3d^7$electrons split into a doubly degenerate e_g band and a triply degenerate t_{2g} band (Fig. 2). The Co^{+2} $3d^7$states, thus, can have two configurations – high spin (HS) state (three electrons up, $S_z = 3/2$) and low spin (LS) state (one electron up, $S_z = 1/2$). We performed calculations of the total energy for both cases, in order to determine the preferential spin state of Co^{+2} in the MgF_2 crystal. Our calculations

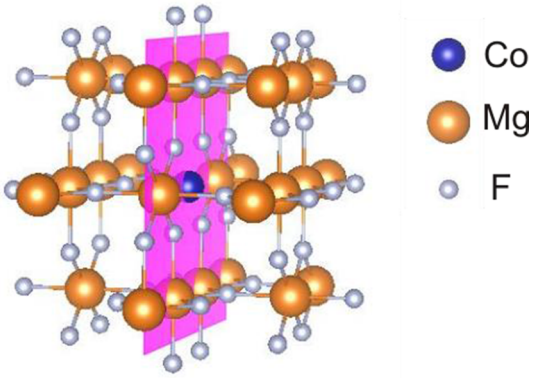

Fig. 1. Model of Co-doped MgF_2 and cross-section plane (shaded) with Miller indices (0 0 1).

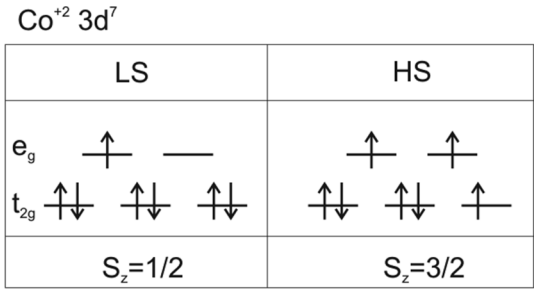

Fig. 2. A schematic representation of the spin distributions in an octahedral crystal field for the low spin (LS) and high spin (HS) states of Co^{+2}. S_z is the spin projection.

Table 6
The calculated (PBEh45) total electronic energy E_{tot} of the Co^{+2}-doped MgF_2 in the high (HS) and low (LS) states. q_{eff}(Co) the effective atomic charge of Co, μ(Co) the magnetic moment of Co, and r the distance between the cobalt ion and the first (second) nearest neighboring fluorine ion. ΔE is the total energy difference between the LS and HS states (per supercell).

Spin state	LS	HS
E_{tot}, a.u.	−12738.4131	−12738.4635
q_{eff}(Co), e	+1.53	+1.53
μ(Co), μ_B	0.95	2.91
r, Å	1.98 (2.04)	2.01 (2.05)
ΔE, eV	1.37	

show, it is the HS state (Table 6) since the total energy of this configuration is considerably lower, by 1.37 eV per supercell. It is consistent with the $^4T_{1a}$ ($t_{2g}^5 e_g^2$) ground state consideration for Co^{+2} in MgF_2 as discussed in [16]. Contrary, it was observed that Co ion in the oxidation state +2 in TiO_2 (in both rutile and anatase structures) is in the LS configuration [35,36]. It should be mentioned that Thienprasert et al. [46] showed that Co ions might form cobalt oxides in TiO_2 in accordance with the XANES measurements. Using the DFT calculations, they found that substitutional Co is preferable, in a comparison with the interstitial Co, under oxygen rich conditions. The substitutional Co might be present in the charge states 0 and −1 (should not be confused with the oxidation state) in this case and, moreover, the local structure changes do not differ for these two charge states. The case of Co^{+2} in MgF_2 is obviously different case, suggesting its interesting behavior in oxides and fluorides.

The relaxation of the CoF_6 octahedron is insignificant in a comparison with the inter-atomic distances of MgF_6 octahedron in pure MgF_2. The distance between Co and 4 F ions (second nearest neighbors) in the same plane (Fig. 1) is 2.01 Å (vs 2.00 Å between Mg and F ions in pure MgF_2). The octahedron is only slightly elongated along the z-direction, i.e. the distance between Co and 2 F ions (first nearest neighbors) is 2.05 Å (vs 1.98 Å between Mg and F ions in pure MgF_2). Note that this conclusion is drawn for the low temperature case. Note that the Mg-F distances do not change in a comparison with the pure MgF_2 crystal even though the presence of Co reduces the symmetry of supercell. Our test calculations for Co substituting for Mg in three different positions in the supercell (site symmetries D_{2h}, C_{2v}, C_s) do not reveal any significant changes as well.

Fig. 3 shows the difference electron density maps for both cases studied – Co^{+2} in the LS and HS states. One can see the electron density redistribution induced by the Co ions. An increase of the difference electron density on the Co ion neighbors is quite obvious and, at least partly, is related to a covalent Co-F bonding. So, the effective atomic charge q_{eff}(F) of the Co first and second (fluorine) nearest neighbors is $-0.825e$ and $-0.830e$, respectively, whereas q_{eff}(F) of other F ions in the supercell is approx. $-0.880e$. In the HS state the far Mg ions (the Co third nearest neighbors) are still perturbed by the Co presence, in

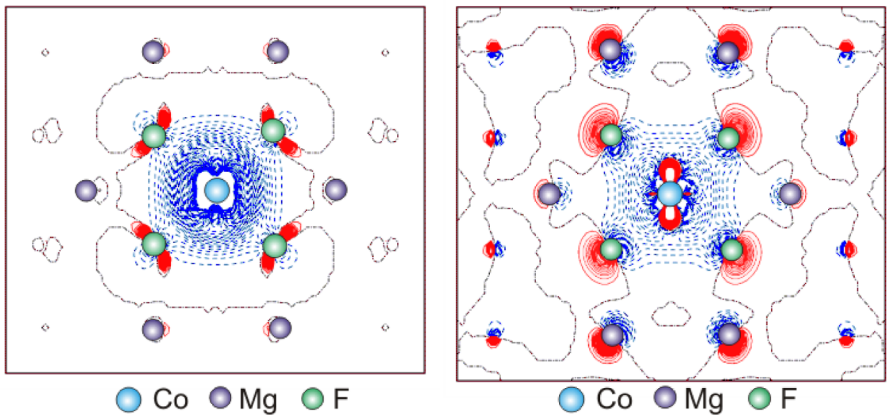

Fig. 3. The difference electron density map for Co^{+2}-doped MgF_2. a) low spin state b) high spin state. On the electron density map, solid (red), dash (blue) and dash-dot (black) lines describe positive, negative and zero values of the induced electron density, respectively. Isodensity increment of 0.002 e a.u.$^{-3}$ (1 a.u. = 1 Bohr). Cross-section plane with the Miller indices (0 0 1). (For interpretation of the references to colour in this figure legend, the reader is referred to the web version of this article.)

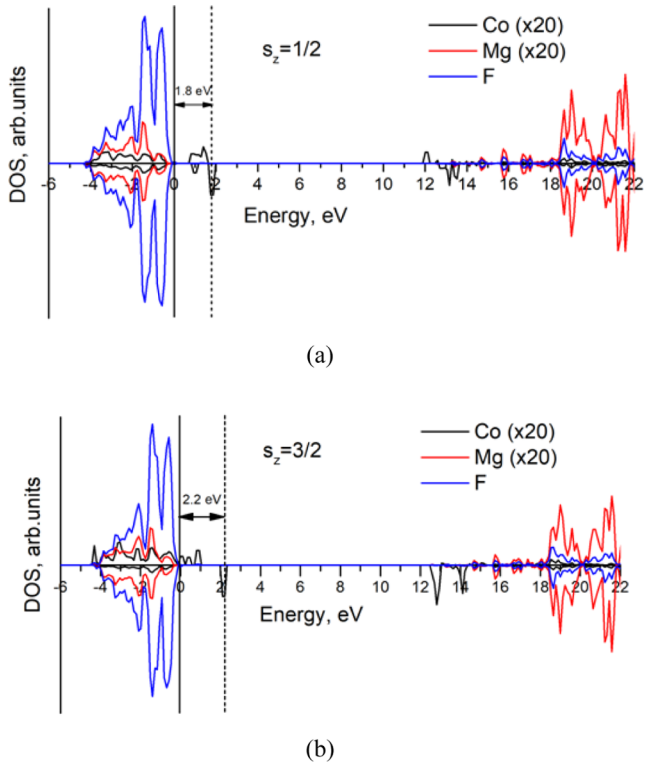

Fig. 4. Electronic density of states (DOS) for Co^{+2} in MgF_2 in (a) the LS state (S_z = 1/2) and (b) HS state (S_z = 3/2). Dashed lines indicate the Fermi level. The negative DOS values correspond to the spin down electrons.

contrast to the LS state, i.e., the electron redistribution extends over much larger area around impurity in the HS state.

The valence band is mainly formed of F states whereas the conduction band is due to Mg states in pure MgF_2. This property is also well seen in the calculated electronic density of states (DOS) in Fig. 4. However, the Co^{+2} ion adds additional peaks in the band gap. Importantly, the additional states of Co^{+2} are observed at 1.8 eV and 2.2 eV (in the spin down channel) from the F 2*p* electrons band maximum for the LS and HS states, respectively. This position of Co^{+2} states is consistent with the experimental data. According to Kappers et al [47] the ground state of Co^{+2} is located not higher than 7 eV above the top of valence band. Thus, the theory allows to fix the ground state energy position at ~2 eV and to position the energy diagram of Co^{+2} in MgF_2 (see Table II in Kappers paper [47]) with respect to the forbidden gap edges.

The additional peaks in the spin-down channel at 1.8 and 2.2 eV for the LS and HS states are understood from the spin-exchange splitting [48]. Thus, analysis of the projection on Co^{+2} ion 3*d* orbitals revealed that the spin-down electrons at 2.2 eV in the HS state (Fig. 4b) occupy the $3d_{xz}$, $3d_{x^2-y^2}$, and $3d_{z^2}$ orbitals. The spin-up electrons of the same orbitals and the $3d_{xy}$ orbital contribute to the three peaks right above the F 2*p* electrons band maximum. Remaining part of the electrons on the 3*d* orbitals of Co^{+2} is hybridized with the electrons of F and Mg between −4 and 0 eV in Fig. 4. In the LS state the spin up and spin down electrons are much less split above the F 2*p* electrons band.

5. Conclusions

The careful hybrid DFT calculations with increased amount of exact non-local exchange were performed for accurate calculations of Co^{+2} impurity in MgF_2 crystals. The band gap for a perfect MgF_2 was reproduced very well in a comparison with experimental data which is important aspect for an analysis of the Co states in the calculated density of states. Moreover, the mechanical properties are also well reproduced. The energetically favourable state of the cobalt atom at low temperatures is a high spin state. Three peaks from the Co atom are seen in the calculated DOS. Moreover, theory allows us to fix the ground state energy position at ~2 eV above the top of valence band and, thus, to position the energy diagram of Co^{+2} in MgF_2 (see Table II in Kappers paper [47]) with respect to the forbidden gap edges.

Declaration of Competing Interest

The authors declare that they have no known competing financial interests or personal relationships that could have appeared to influence the work reported in this paper.

Acknowledgements

This research was partly supported by the Kazakhstan Science Project № AP05134367«Synthesis of nanocrystals in track templates of SiO_2/Si for sensory, nano- and optoelectronic applications», as well as by Latvian Research Council project lzp-2018/1-0214.

Calculations were performed on Super Cluster (LASC) in the Institute of Solid State Physics (ISSP) of the University of Latvia. Authors are indebted to S. Piskunov for stimulating discussions.

References

[1] W.F. Hanson, E.T. Arakawa, M.W. Williams, J. Appl. Phys. 43 (4) (1972) 1661–1665.
[2] J. Thomas, G. Stephan, J.C. Lemonnier, M. Nisar, S. Robin, Phys. Status Solidi (b) 56 (1) (1973) 163–170.
[3] P. Laporte, J.L. Subtil, M. Courbon, M. Bon, L. Vincent, JOSA 73 (8) (1983) 1062–1069.
[4] D. Einfeld, K. Grützmacher, D. Stuck, Zeitschrift für Naturforschung A 34 (2) (1979) 233–238.
[5] A. Bideau-Mehu, Y. Guern, R. Abjean, A. Johannin-Gilles, J. Phys. E: Sci. Instrum.

13 (11) (1980) 1159.
[6] V.B. Voloshinov, N. Gupta, Appl. Opt. 45 (13) (2006) 3127–3135.
[7] L.F. Johnson, R.E. Dietz, H.J. Guggenheim, Appl. Phys. Lett. 5 (2) (1964) 21–22.
[8] M.P. Frolov, Y.P. Podmar'kov, Opt. Commun. 155 (4–6) (1998) 313–316.
[9] R. DeSalvo, A. Said, D.J. Hagan, E.W. Van Stryland, M. Sheik-Bahae, Quantum Electronics, IEEE J. Quantum Electron. 32 (1996) 1324–1333.
[10] F. Nakamura, T. Kato, G. Okada, N. Kawaguchi, K. Fukuda, T. Yanagida, Ceram. Int. 43 (9) (2017) 7211–7215.
[11] F. Nakamura, T. Kato, G. Okada, N. Kawano, N. Kawaguchi, K. Fukuda, T. Yanagida, Mater. Res. Bull. 98 (2018) 83–88.
[12] L.B. Lapson, J.G. Timothy, Appl. Opt. 15 (5) (1976) 1218–1221.
[13] L.N. Feuerhelm, W.A. Sibley, J. Phys. C: Solid State Phys. 16 (4) (1983) 799.
[14] Y. Suzuki, W.A. Sibley, O.H. El Bayoumi, T.M. Roberts, B. Bendow, Phys. Rev. B 35 (9) (1987) 4472.
[15] R. Moncorge, F. Auzel, J.M. Breteau, Philos. Mag. B 51 (5) (1985) 489–499.
[16] H. Manaa, Y. Guyot, R. Moncorge, Phys. Rev. B 48 (6) (1993) 3633.
[17] V.M. Lisitsyn, L.A. Lisitsyna, A.I. Popov, E.A. Kotomin, F.U. Abuova, A. Akilbekov, J. Maier, Nucl. Instrum. Methods B 374 (2016) 24–28.
[18] V.N. Kuzovkov, E.A. Kotomin, A.I. Popov, Nucl. Instrum. Methods B 435 (2018) 79–82.
[19] A. Dauletbekova, F. Abuova, A. Akilbekov, E. Kotomin, S. Piskunov, Phys. Status Solidi C 10 (2) (2013) 160–164.
[20] V. Lisitsyn, L. Lisitsyna, A. Dauletbekova, M. Golkovskii, Z. Karipbayev, D. Musakhanov, E. Polisadova, Nucl. Instrum. Methods B 435 (2018) 263–267.
[21] A.S. El-Said, R. Neumann, K. Schwartz, C. Trautmann, Nucl. Instrum. Methods B 245 (1) (2006) 250–254.
[22] R. Dovesi, V.R. Saunders, C. Roetti, R. Orlando, C.M. Zicovich-Wilson, F. Pascale, B. Civalleri, K. Doll, N.M. Harrison, I.J. Bush, Ph. D'Arco,M. Llunell, M.Causá and Y. Noël, CRYSTAL14 User's Manual University of Torino, Torino, Italy. http://www.crystal.unito.it/.
[23] J.P. Perdew, M. Ernzerhof, K. Burke, J. Chem. Phys. 105 (1996) 9982.
[24] J. Heyd, G.E. Scuseria, M. Ernzerhof, J. Chem. Phys. 118 (18) (2003) 8207-8215. Correction: J. Heyd, G. E. Scuseria, M. Ernzerhof, J. Chem. Phys., 124 (2006) 219906.
[25] M.I. McCarthy, N.M. Harrison, Phys. Rev. B 49 (1994) 8574.
[26] M. Catti, R. Dovesi, A. Pavese, V.R. Saunders, J. Phys.: Condens. Matter 3 (1991) 4151.
[27] M. Dolg, U. Wedig, H. Stoll, H. Preuss, J. Chem. Phys. 86 (1987) 866.
[28] J.M.L. Martin, A. Sundermann, J. Chem. Phys. 114 (2001) 3408.
[29] R.S. Mulliken, J. Chem. Phys. 23 (10) (1955) 1833.
[30] H.J. Monkhorst, J.D. Pack, Phys. Rev. B 13 (1976) 5188.
[31] R.A. Evarestov, Quantum Chemistry of Solids vol. 153, (2012) 734.
[32] M. Ferrero, M. Rérat, R. Orlando, R. Dovesi, J. Chem. Phys. 128 (2008) 014100.
[33] M. Ferrero, M. Rérat, R. Orlando, R. Dovesi, J. Comput. Chem. 29 (2008) 1450.
[34] M. Ferrero, M. Rérat, R. Orlando, R. Dovesi, J. Chem. Phys. 129 (2008) 244110.
[35] W. Yan, Z. Sun, T. Yao, Z. Pan, Z. Li, Q. Liu, S. Wei, J. Appl. Phys. 106 (2009) 123918.
[36] H. Weng, J. Dong, T. Fukumura, M. Kawasaki, Y. Kawazoe, Phys. Rev. B 73 (2006) 121201(R).
[37] A.F. Fix, F.U. Abuova, R.I. Eglitis, E.A. Kotomin, A.T. Akilbekov, Phys. Scr. 86 (2012) 030504.
[38] M. Catti, A. Pavese, R. Dovesi, C. Roetti, M. Causa, Phys. Rev B. 44 (1991) 8.
[39] A.S. Barker, Phys. Rev. 136 (1964) 5A.
[40] W.F. Perger, J. Criswell, B. Civalleri, R. Dovesi, Comput. Phys. Commun. 180 (2009) 1753–1759.
[41] C. Franchini, J. Phys.:Condens. Matter 26 (2014) 253202.
[42] D. Du, M.J. Wolf, K. Hermansson, P. Broqvist, Phys. Rev. B 97 (2018) 235203.
[43] F. Oba, A. Togo, I. Tanaka, J. Paier, G. Kresse, Phys. Rev. B 77 (2008) 245202.
[44] A. Kuzmin, A. Kalinko, R.A. Evarestov, Acta Mater. 61 (2013) 371.
[45] C.A. Guido, E. Brémond, C. Adamo, P. Cortona, J. Chem. Phys. 138 (2013) 021104.
[46] J.T. Thienprasert, S. Klaithong, A. Niltharach, A. Worayingyong, S. Na-Phattalung, S. Limpijumnong, Curr. Appl. Phys. 11 (2011) S279.
[47] L.A. Kappers, S.I. Yun, W.A. Sibley, Phys. Rev. Lett. 29 (1972) 943.
[48] H.-X. Deng, J. Li, S.-S. Li, J.-B. Xia, A. Walsh, S.-H. Wei, Appl. Phys. Lett. 96 (2010) 162508.